https://doi.org/10.5194/egusphere-2026-4740
Preprint. Discussion started: 28 August 2026

Explaining observed surface radiation trends 2001-2023 on Alaska's North Slope

Leah J. Bertrand[1,2], Jennifer E. Kay[1,2], and Gijs de Boer[3]

[1]Department of Atmospheric and Oceanic Sciences, University of Colorado at Boulder, Boulder, CO, United States of America
[2]Cooperative Institute for Research in Environmental Sciences, Boulder, CO, United States of America
[3]Environmental Science and Technologies Department, Brookhaven National Laboratory, Upton, NY, USA

Correspondence: Leah J. Bertrand (leah.bertrand@colorado.edu), Jennifer E. Kay (jennifer.e.kay@colorado.edu), and Gijs de Boer (gdeboer@bnl.gov)

Abstract. Changes in surface radiation are a key contributor to Arctic surface warming. However, the details of Arctic surface radiation change are not fully known due to a lack of multi-decadal observations. Here, we leverage 23 years (2001-2023) of ground-based observations at two neighboring coastal tundra sites on the North Slope of Alaska (NSA) to explain surface radiation change. US Department of Energy Atmospheric Radiation Measurement (ARM) and National Oceanic and Atmospheric Administration (NOAA) facilities in Utgiagvik, Alaska have documented warming (0.9 K/decade since 2001) and surface radiation change. Surface downwelling longwave radiation increases year-round. Surface downwelling and net shortwave radiation decrease during sunlit months (April-September). Decreasing net shortwave radiation is driven by changing cloud properties and increasing surface albedo over exposed tundra in mid-summer. Increasing downwelling longwave radiation during both sunlit and dark months (October-March) is driven by atmospheric warming, increasing water vapor, and changing cloud properties. Atmospheric warming and increasing water vapor explain about half the total observed increase in downwelling longwave radiation, while changing cloud properties explain the rest. Assessed cloud drivers (liquid water path, cloud cover, and low cloud fraction) explain increasing longwave radiation during sunlit months but are insufficient during dark months. Changes in assessed cloud drivers increased longwave radiation in all seasons except SON, when there was no change. These results reveal substantial surface radiative changes on the NSA, where cloud radiative effect changes amplify surface warming during dark months and dampen it during sunlit months.

1 Introduction

The Arctic has warmed more than anywhere else in the world over recent decades, several times the global average (Zhou et al., 2024). This phenomenon, known as Arctic amplification, is widely documented in both earth system model (ESM) simulations and observations, manifesting as near-surface air temperature increases that far outpace the global average. This amplified warming arises because radiative feedbacks are more positive in the Arctic than elsewhere: as the Arctic system responds to perturbations, the resulting changes trap more radiation and thus require additional warming to restore equilibrium. Although the dominant factors driving Arctic amplification have been understood since the early days of global climate models,

https://doi.org/10.5194/egusphere-2026-4740
Preprint. Discussion started: 28 August 2026

present-day ESMs still disagree widely on its magnitude. This disagreement comes from differences in the modeled radiative importance of various atmospheric, surface, and ocean processes. Observations can provide insight into this disagreement by indicating the radiative processes most important for early 21st-century Arctic warming.

One feedback which is particularly difficult to constrain is the radiative effect of cloud changes. This difficulty arises from unique Arctic conditions which challenge models (e.g., Korolev et al., 2017) and satellite retrievals (Graham et al., 2017; Liu et al., 2017; Wang et al., 2021; Liu et al., 2022; Huang et al., 2022; Barrientos-Velasco et al., 2025). Due to the prevalence of thin clouds (Turner et al., 2007), high surface albedo, and minimal sunlight, Arctic cloud changes can radiatively warm or cool depending on a whole host of factors (e.g., Shupe and Intrieri, 2004). This situation is more complex than the mid-latitudes, where low surface albedo and substantial sunlight mean that cloud cover or liquid water path increases radiatively cool (e.g., Ceppi et al., 2016; Zelinka et al., 2020). Ground-based observatories evade some of these difficulties via accurate observations of the lower atmosphere, making them a useful tool for constraining Arctic surface cloud radiative effects at a single location.

Surface radiative effects matter because Arctic warming is greatest near the surface. However, fully understanding drivers of surface warming requires knowledge of the surface energy budget. The surface energy budget consists of many components depending on the surface type considered, but it can generally be divided into atmospheric forcing and surface response terms. Atmospheric forcing terms consist of downwelling longwave radiation and net (i.e., absorbed) shortwave radiation. The response terms are upwelling longwave radiation, directly related to surface skin temperature, along with turbulent and conductive heat fluxes (e.g., Miller et al., 2017; Solomon et al., 2023; Sledd et al., 2025). The atmospheric forcing terms describe radiant energy input to the surface by the atmosphere, while the response terms describe the resultant effects of a change in forcing. Outside of melt conditions, about half of the change in the atmospheric forcing goes into changing surface skin temperature over a variety of Arctic surface types (Miller et al., 2017; Sledd et al., 2025).

Observations of the full Arctic surface energy budget are invaluable but limited in time. Observing any environmental change over time generally requires decades of observations. Some locations in the Arctic have decades of observations of the radiative portion of the surface energy budget. Several high Arctic research stations have measured the full surface radiation budget for 2-3 decades. Surface radiation includes the atmospheric forcing terms as well as a single response term, upwelling longwave radiation. Examining change to the surface radiation budget outlines changes in the atmospheric forcing and part of the surface response.

One such site is the Atmospheric Radiation Measurement (ARM) program's North Slope of Alaska (NSA) facility (Verlinde et al., 2016) near Utqiagvik, Alaska. It has taken decades of detailed observations in the context of substantial local warming (Dong et al., 2010). On the coast of the Beaufort Sea, NSA lies adjacent to an area of substantial sea ice loss (Stroeve et al., 2012). Other decadal changes are observed, such as springtime snowmelt becoming earlier over 1979-2016 (Stone et al., 2002; Cox et al., 2017) and summer greening over the broader North Slope (Wu et al., 2020; Plekhanova et al., 2022). Furthermore, a neighboring NOAA facility takes separate measurements of the surface radiation budget, enabling verification of results.

Ground-based observations from ARM NSA have recorded surface radiation changes over the 21st century, as have other long-term Arctic observatories. Increasing surface downwelling longwave radiation has been noted during winter at a European Arctic observatory (Maturilli et al., 2015). Increasing downwelling longwave radiation has also been noted during all seasons

https://doi.org/10.5194/egusphere-2026-4740
Preprint. Discussion started: 28 August 2026

at ARM NSA (Bertossa and L'Ecuyer, 2025), though the magnitude of the increase has a pronounced seasonal cycle. Broadly, the seasonal cycle of Arctic radiation can be grouped into months with less warming and more sunlight ('sunlit months' AMJJAS) and months with more warming and less sunlight ('dark months' ONDJFM). Downwelling longwave radiation has a greater increase during dark than sunlit months, consistent with the seasonality of Arctic warming (e.g., Screen et al., 2012). At ARM NSA, increasing wintertime longwave radiation was attributed to changing cloud properties, atmospheric warming, and increasing water vapor (Bertrand et al., 2025; Riot-Bretêcher et al., 2025). In terms of shortwave radiation, a decrease during July and August has been noted, with increasing cloud liquid water path suggested as a driver (Lubin et al., 2026). However, radiation change is often reported without a quantitative attribution of its drivers. Knowledge of which surface and atmospheric properties drove the change is essential for identifying the most radiatively impactful processes. To the authors' knowledge, no study has used Arctic ground-based observations to attribute drivers of changing surface shortwave radiation or changing longwave radiation during non-winter months.

Quantitative assessment of drivers of radiation change is challenging because radiation has a complex dependence on a number of atmospheric and surface properties. The vertical structure of temperature, greenhouse gases, and clouds all impact longwave radiation. Shortwave radiation is affected by surface albedo, solar zenith angle, clouds, water vapor, and other trace gases. Estimates of all of these quantities over a study period are necessary to assess the radiative impact of a possible change. The aim of this paper is to quantitatively link observed surface radiation change to observed surface and atmospheric property changes.

In this study, we attribute drivers of radiation change at NSA 2001-2023 and find a large impact of cloud radiative changes as well as an effect from increasing surface albedo during mid-summer. We find that cloud shortwave cooling increases during sunlit months while cloud longwave warming increases during dark months. During sunlit months, clouds and increasing surface albedo completely reverse the longwave warming effect of increasing water vapor and atmospheric temperature. During dark months, clouds double the surface longwave warming effect of increasing atmospheric temperatures and water vapor.

2 Methods

This study consists of three components. First, we analyze temporal changes to surface radiation and radiatively important properties ('drivers'). Next, we derive simplified radiative kernels from radiative transfer calculations based on ARM NSA observations. Finally, we use these kernels to reconstruct radiative anomalies and attribute radiation change to specific drivers.

2.1 Data

The Utqiagvik site has the unique benefit of two independent surface radiation observing platforms. ARM and NOAA both maintain calibrated and quality-controlled observations of the surface radiation budget within close proximity. Observational records start in the 1990s, but we only consider data collected after 2001, when calibrated microwave radiometer retrievals began. We do not consider data after 2023 because this was the most recent available year of calibrated microwave radiometer retrievals when analysis was conducted.

https://doi.org/10.5194/egusphere-2026-4740
Preprint. Discussion started: 28 August 2026

Surface radiation is measured by a combination of pyrgeometer, pyranometer, and pyrheliometer. We use quality-controlled 1-minute data from both ARM and NOAA sites from the QCRAD product (Table 1). Longwave fluxes are measured directly by pyrgeometers, while shortwave fluxes rely on different combinations of instruments for upwelling and downwelling radiative fluxes. For downwelling shortwave radiation, we use the sum of direct and diffuse radiation measurements from a pyrheliometer and shaded pyranometer. ARM QCRAD data uses unshaded pyranometer measurements when the shortwave radiation sum is not available, while NOAA data only uses the shortwave radiation sum. To identify radiation observations with hemispheric clear skies, we use the method of (Riihimaki et al., 2003). This method relies on temporal variations in downwelling longwave and shortwave radiation. It generally captures ceilometer-cloudy conditions along with partly cloudy scenes which would otherwise be missed.

Prior to trend analysis, radiation observations are averaged to monthly temporal frequency. Monthly averages for longwave radiation and downwelling shortwave radiation are retained when over 75% of underlying data points are assessed to be of good quality. Net shortwave radiation is then calculated from monthly-mean albedo and downwelling shortwave radiation according to $F_{sw}^{N} = (1-\alpha)F_{sw}^{\downarrow}$. Surface albedo is calculated from 1-minute upwelling and downwelling shortwave radiation when the following condition is met:

$$F_{sw}^{\uparrow} < 0.9F_{sw}^{\downarrow} + 25\ \mathrm{W/m^2}, \quad F_{sw}^{\downarrow} > 50\ \mathrm{W/m^2}, \tag{1}$$

where $F_{sw}^{\uparrow}$ refers to upwelling shortwave radiation and $F_{sw}^{\downarrow}$ to direct plus diffuse shortwave. This condition was proposed by Long and Shi (2006) and reduces unphysical albedo values during low-sunlight conditions. We then mask data points below 0 or above 1 and take the average of resulting observations. Monthly-mean albedo is reported when over 25% of underlying data points are of good quality. We chose this lower threshold because of the data reduction implied by (1). When the 25% threshold is not met, we fill monthly-mean albedo with its climatological value. This value is defined as the average of all valid observations during each month over the entire record. No climatological value is available during December and January due to downwelling shortwave radiation never exceeding 50 W/m^2. During these months, we stipulate an albedo of 0.8 corresponding to snow. We fill monthly-mean surface albedo with its climatology rather than interpolating so as not to impact trend analysis.

Cloud properties are measured using a suite of ground-based instruments at ARM NSA. For our radiative transfer calculations, we use the Shupe-Turner cloud microphysics product (Shupe et al., 2015). This product is a combination of observations from radar, lidar, ceilometer, infrared spectrometer, microwave radiometer, and radiosondes. It retrieves vertical profiles of cloud ice and liquid water path along with effective ice crystal and liquid droplet radii. However, the Shupe-Turner product only covers 11 of the 23 study years and so cannot be used directly for attribution analysis of change over time.

For analysis of change over time, we rely on lower-level cloud observations with full 2001-2023 coverage. We use cloud cover and low cloud fraction (defined as cloud base height $<$ 250 m) based on ceilometer retrievals. Cloud cover is defined as when the ceilometer detects significant backscatter. We use liquid water path retrieved from a microwave radiometer (Table 1). We mask liquid water path observations when no cloud is detected by ceilometer. No cloud ice water path or cloud phase retrievals were used since no data products were identified with 23-year coverage.

https://doi.org/10.5194/egusphere-2026-4740
Preprint. Discussion started: 28 August 2026

Physical quantities	Primary instrument	Citation
Hemispheric downwelling shortwave flux (direct plus diffuse)	Pyrheliometer, shaded pyranometer	Zhang (1998)
Hemispheric downwelling longwave flux	Pyrgeometer	Zhang (1998)
Cloud liquid water path, precipitable water vapor	Two-channel microwave radiometer	Zhang (2002)
Cloud cover, cloud base height	Ceilometer	Morris et al. (1997)
Near-surface air temperature	Surface meteorological instrumentation	Kyrouac et al. (2003)

Table 1. Long-term data products (2001-2023) used for radiation driver analysis.

Non-cloud atmospheric properties are measured using radiosondes, surface meteorological instrumentation, two-channel microwave radiometer, and chemical analysis (Table 1). Near-surface air temperature is measured by surface meteorological instrumentation. Precipitable water vapor is retrieved from a microwave radiometer according to Zhang (2002). CO_2 concentration is calculated from NOAA flask sampling. Radiosonde data are only used for radiative transfer calculations.

2.2 Radiative transfer calculations

Estimates of the radiative effect of anomalies in each driver are necessary to explain radiation change. To this effect, we conduct perturbations of a single driver in profiles of ARM NSA observations supplied to a radiative transfer model. Our radiative transfer calculations are based on the ARM NSA observations themselves, thus removing any mean-state biases usually imported through the use of model-based radiative kernels (e.g., Zhou et al., 2022). This unique approach offers an accurate climate mean state about which to evaluate radiation sensitivity to change.

Calculations are performed in a manner consistent with previous radiative closure exercises at ARM NSA (Shupe et al., 2015; Bertrand et al., 2025). Radiative transfer calculations for both longwave and shortwave radiation are completed with the Rapid Radiative Transfer Model (RRTM) (Mlawer et al., 1997), a validated correlated-k code widely used in atmospheric sciences (Clough et al., 2005). We create profiles from individual radiosonde launches by averaging Shupe-Turner microphysics for a 31-minute window centered on sonde launch time. When an individual radiosonde ends, we fill with the average profile of temperature and humidity for that month. Above 20 km, we fill with standard profiles for sub-Arctic summer during June-September and sub-Arctic winter otherwise. We use these standard profiles to supply all trace gases other than CO_2 and ozone. CO_2 profiles are vertically constant and given by NOAA flask measurements. O_3 profiles are supplied from the grid box of Rosenlof et al. (2015) nearest to ARM NSA scaled to satellite-retrieved total column ozone from Smith and Barnet (2023). No aerosols are included in radiative transfer calculations.

We then perturb a single driver for every valid profile in RRTM, running both longwave and shortwave radiation variants. Several assumptions are needed in order to translate our near-surface or column-integrated drivers into vertical perturbation profiles. For temperature, we use the radiosonde-observed vertical structure of temperature anomalies corresponding to a given near-surface air temperature anomaly. For water vapor, we use the observed vertical structure of water vapor mixing ratio anomalies observed by radiosonde corresponding to a given precipitable water vapor anomaly. These mappings are calculated

https://doi.org/10.5194/egusphere-2026-4740
Preprint. Discussion started: 28 August 2026

for each month separately in order to account for the seasonal cycle of water vapor. For liquid water path, we uniformly scale liquid water content to match a given liquid water path anomaly. For cloud cover, we rely on cloud radiative effect (CRE) calculated from setting cloud condensate equal to zero. For low cloud fraction, we use an empirical approach rather than radiative transfer calculations.

2.3 Driver attribution

Once radiative transfer perturbation calculations are complete, we derive simplified radiative kernels. Instead of specifying radiation sensitivity to a driver on a 2D grid of cloud optical depth and cloud top height, we specify the sensitivity under four cloud conditions – clear-skies, ice-only clouds, mixed-phase clouds, and liquid-only clouds. The impacts of anomalies in air temperature, water vapor, and CO_2 are then considered to be linear within each state according to

$$\Delta F_j|_{\Delta x} = \sum_k K_j(x_k)\Delta n(x_k) \approx \frac{\partial F_j}{\partial x}\Delta x \;\; \text{if} \;\; x \neq \text{cloud driver}, \tag{2}$$

where F_j indicates the broadband irradiance for atmospheric state j (j =clear-skies, ice-only clouds, mixed-phase clouds, liquid-only clouds), $K_j(x_k)$ indicates the radiative kernel for driver x in atmospheric state j resolved by driver bin k, $\Delta n(x_k)$ indicates the normalized histogram of driver x by bin k, $\partial F_j/\partial x$ indicates the sensitivity of radiation to a change in the average value of x, and Δx indicates monthly-mean anomalies in driver x.

Cloud properties are treated differently due to the non-linear relationships between cloud properties and radiation. For liquid water path (LWP), $K_j(x_k)$ is calculated from the average CRE for a given water path bin. CRE is calculated in a radiative transfer model by setting cloud cover to zero. For longwave radiation, CRE-LWP distributions are estimated from minute-by-minute radiative transfer calculations in cloudy skies with cloud cover set to zero. For shortwave radiation, CRE-LWP distributions are estimated from sweeps of liquid water path perturbations of individual radiosonde-microphysics profiles. For each set of liquid water path perturbations on a profile, we fit a curve of the form

$$F_{sw}^{\downarrow} = F_{sw,clr}\left(1 - \frac{b_0 WP}{1 + b_0 WP}\right), \tag{3}$$

to the result, where WP is liquid water path and $F_{sw,clr}$ and b_0 are parameters to fit. Note that shortwave CRE is $F_{sw}^{\downarrow} - F_{sw,clr}$. The form of this curve was specified in Stephens (1978) and Shupe and Intrieri (2004). Then the average CRE from all fitted curves in each LWP bin for each cloud phase is $K_j(x_k)$.

The radiative effect of cloud cover anomalies also requires a different approach. Cloud cover cannot be specified as driver x_k in (2) because cloud cover anomalies are a change in the weights f_j. Cloud cover is only an effect on the all-sky radiation F because of changes in the frequency of states j, rather than a change in the radiation within the state j. Cloud cover as a driver is described as the effect of a change in w_{clr} on the all-sky radiation F_{allsky} as

$$\Delta F_{\text{allsky}} = \sum_j w_j \Delta F_j + \frac{\partial F_{\text{allsky}}}{\partial w_j}\Delta w_j, \tag{4}$$

https://doi.org/10.5194/egusphere-2026-4740
Preprint. Discussion started: 28 August 2026

where w_j is the frequency of atmospheric state j. Note that $F_{\text{allsky}} = \sum_j w_j F_j$. Sensitivities $\frac{\partial F_{\text{allsky}}}{\partial w_j}$ are calculated from the average difference in observations between F_j and F_{allsky}.

Since long-term information on the frequency of cloud phase is not available, we assume the cycle of $w_{j \neq clr}$ scaled by the observed cloud cover. The scalar sensitivity $\partial F_{\text{allsky}} / \partial w_j$ is calculated from the mean difference between cloudy and clear observations. Note that all kernels/sensitivities are calculated separately by longwave vs. shortwave, month, and atmospheric state j. This way, the assumed mean state about which perturbations are taken always includes the seasonal cycle.

Finally, the relationship between low cloud fraction and radiation also required a tailored approach. We define the radiative sensitivity to be the difference in downwelling longwave radiation between low and non-low (cloud base height $>$ 250 m) clouds after controlling for variations in liquid water path. This 250 m threshold was chosen because observations only show a relationship between cloud base height and radiation for the lowest layers of the atmosphere (Fig. A1). These tailored approaches allow us to attribute radiative anomalies to specific drivers while relying on local observations.

3 Results

3.1 Observed surface radiation changes

The seasonal cycle of surface radiation (Fig. 1a) at the two sites (ARM and NOAA) shows two distinct regimes. During dark months (October to March), the energy budget is longwave-driven. Due to little insolation and high surface albedo, there is minimal absorption of shortwave radiation ($\leq$20 W/m^2). Downwelling longwave radiation, meanwhile, is an order of magnitude larger ($\approx$200 W/m^2). During sunlit months (April to September), net shortwave makes up a substantial component of the surface energy budget, peaking in June and July around 160 W/m^2. Increased sunlight is accompanied by rising downwelling longwave radiation, which grows by 50% between the dark season minimum and the sunlit season maximum in August.

Within this strong seasonal cycle, downwelling longwave radiation is increasing and net shortwave radiation is decreasing (Fig. 1b). Between the first (2001-2010) and last (2014-2023) decade of observations, both longwave and shortwave radiation changed. Downwelling longwave radiation increased during both sunlit and dark seasons. Net shortwave radiation decreased during the sunlit season, with little to no change during the dark season. Differences between 2001-2010 and 2014-2023 are as large as 20 W/m^2, highlighting substantial variations over the course of decades.

The two independent radiation records agree about the sign, magnitude, and seasonality of radiation differences over time. Both sites show increased longwave radiation during many months of the year, in addition to agreeing on no change during April and September. ARM and NOAA both show decreased net shortwave radiation from May to August. Net shortwave decreases are of similar magnitude during the sunlit season. Both sites show minimal shortwave changes during the dark season. The consistency between sites gives confidence in radiation changes at ARM NSA.

Trend analysis (Fig. 2) reveals increasing downwelling longwave radiation and decreasing net shortwave radiation. Downwelling longwave radiation increases during both sunlit and dark months, with a stronger increase during the dark season. Net shortwave radiation decreases during the sunlit season and has no change during the dark season. During sunlit months, these

https://doi.org/10.5194/egusphere-2026-4740
Preprint. Discussion started: 28 August 2026

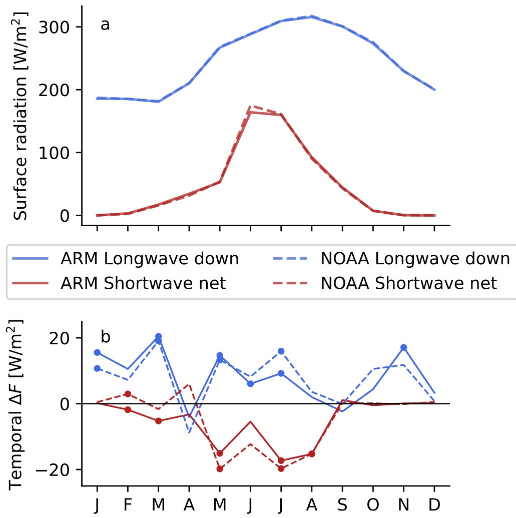

Figure 1. Downwelling longwave and net shortwave (a) seasonal cycle and (b) difference between 2014-2023 and 2001-2010 at ARM NSA facility (solid) and neighboring NOAA Atmospheric Baseline Observatory (dashed). Significant ($\alpha = 0.1$) differences between first and last decade of observations indicated by markers in (b), determined using a two-sided t-test.

opposing radiation changes cancel out in terms of the total radiation input. The total radiation input to the surface is stable in ARM observations and decreasing in NOAA observations.

While ARM and NOAA observations agree on many radiative changes, there is some disagreement in terms of their precise magnitude. Both sites agree on the sign and significance of longwave and shortwave radiative changes during both sunlit and dark months. During sunlit months, however, NOAA shows a decrease in net shortwave radiation nearly double the magnitude of the decrease in ARM data. As a result, ARM total radiation input is stable while it is decreasing at the NOAA site. Yet no difference is apparent when considering downwelling shortwave radiation–agreement is strong (Fig. A2). Instead, the difference results from the earlier melt-out date at the NOAA site (Fig. 5a), creating a larger net impact of the decrease in incoming shortwave.

In contrast, downwelling longwave radiation trends agree well. During sunlit months, the mean value and spread of the increases are similar. During dark months, ARM data shows a slightly larger increase in downwelling longwave radiation, though their magnitudes are broadly consistent. The comparison between two independent radiation records gives us confidence in the sign of longwave and shortwave radiative trends while acknowledging spread in their precise magnitude and sum.

Surface skin temperature at NSA is also changing. Surface skin temperatures increase during dark months while remaining stable during sunlit months (Fig. 3). The seasonality and magnitude of surface skin temperature trends are nearly the same in ARM and NOAA observations, with a strong increase during dark months and no increase during sunlit months. Broadly, surface skin temperature follows changes in radiation input to the surface. During dark months, increasing total radiation input to the surface is consistent with surface warming. During sunlit months, stable total radiation input is consistent with stable

https://doi.org/10.5194/egusphere-2026-4740
Preprint. Discussion started: 28 August 2026

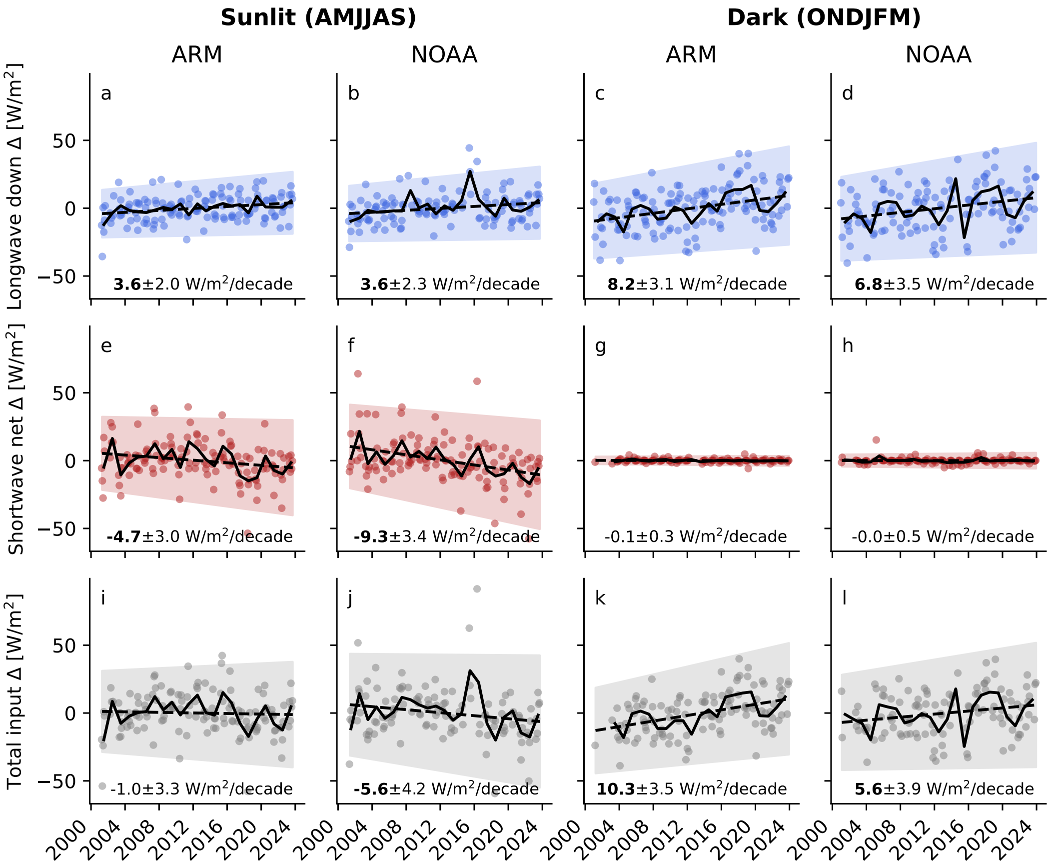

Figure 2. (a-d) Downwelling longwave radiation, (e-h) net shortwave radiation, and (i-l) total radiation input to the surface (longwave plus shortwave) over time at ARM and NOAA sites in Utqiagvik separated by sunlit and dark months. Markers indicate monthly-mean anomalies and solid line indicates 6-month average. Line of best fit is indicated by dashed line and shaded area indicates 90% confidence band, calculated from monthly means using ordinary least squares regression. Text indicates trend, with significance at the 90% confidence level (according to Student's t-test) indicated by bolding.

surface skin temperatures. The exception is sunlit months in NOAA observations: surface skin temperatures are stable despite decreasing total radiation input. In either case, we see that ARM and NOAA surface skin temperatures do not increase during sunlit months despite increasing downwelling longwave radiation.

3.2 Radiation driver trends

Surface radiation change is driven by changes in atmospheric, cloud, and surface properties. Below, we examine changes in observations of radiatively important properties (drivers) to contextualize radiation change in Utqiagvik, AK. We assess air temperature, water vapor, surface albedo, cloud cover, cloud liquid water path, and low cloud fraction as drivers. What follows

https://doi.org/10.5194/egusphere-2026-4740
Preprint. Discussion started: 28 August 2026

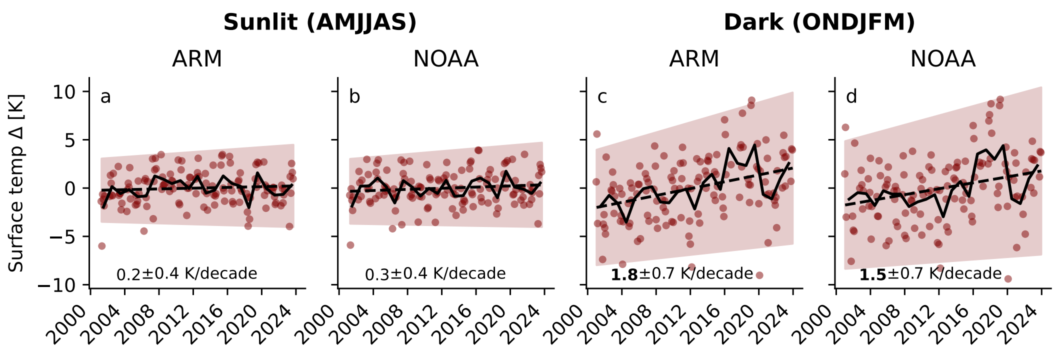

Figure 3. Like Figure 2, but for surface skin temperature calculated from upwelling longwave radiation assuming unity emissivity.

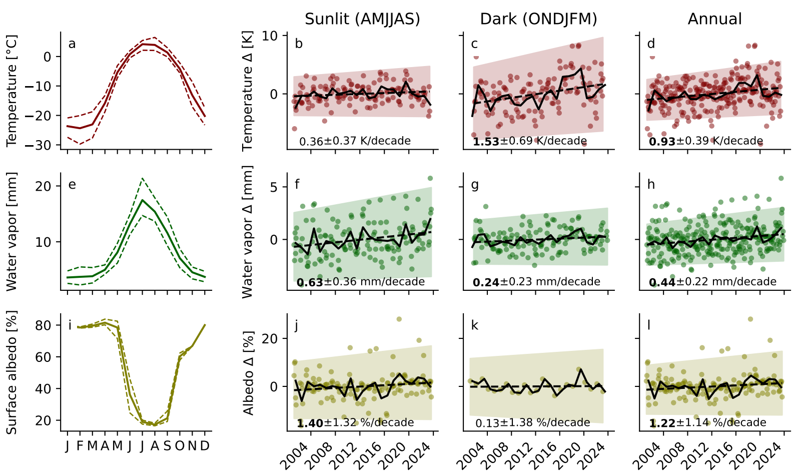

Figure 4. Seasonal cycle (a,f,k) and time series of radiatively important non-cloud properties at ARM NSA facility 2001-2023 by 'sunlit' (c,h,m), 'dark' (d,i,n), and annually (e,j,o). Properties are near-surface air temperature (top row), precipitable water vapor (middle row), and surface albedo (bottom row). For seasonal cycle panels, solid line is the average and dashed lines are 10th and 90th percentiles for monthly-mean anomalies. For time series panels, markers indicate monthly-mean anomalies and solid line indicates seasonal (or annual) average. Line of best fit is indicated by dashed line and shaded area indicates 90% confidence band, calculated from monthly means using ordinary least squares regression. Text indicates trend, with significance at the 90% confidence level (according to Student's t-test) indicated by bolding.

is based primarily on ARM NSA data because the NOAA site has somewhat less extensive observations of radiatively important atmospheric properties.

Observations at ARM NSA reveal atmospheric warming and moistening within a pronounced seasonal cycle (Fig. 4). Near-surface air temperature increases from -23 °C at its minimum in February up to 4.2 °C at its maximum in July. Within this seasonal cycle, near-surface air temperature increases by 1.53±0.69 °C/decade (90% confidence interval) during dark months ($p < 0.01$). By comparison, sunlit months have a modest increase of 0.36±0.37 °C/decade ($p = 0.11$). Precipitable water vapor

https://doi.org/10.5194/egusphere-2026-4740
Preprint. Discussion started: 28 August 2026

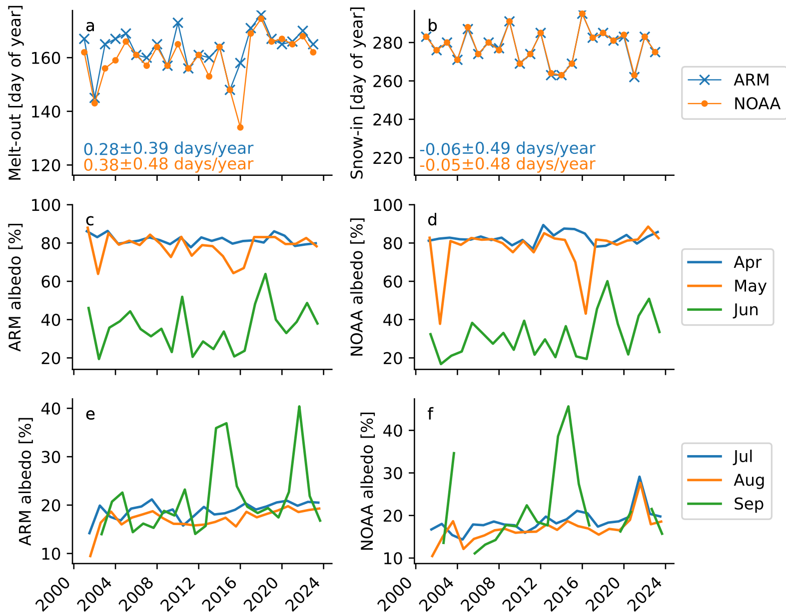

Figure 5. Melt-out and snow-in dates determined from daily ARM and NOAA albedo data (top row) using the method of Cox et al. (2017). Monthly-mean surface albedo in April, May June (middle row) and July, August, September (bottom row) at ARM (left column) and NOAA (right column) sites. Line of best fit is indicated by dashed line and shaded area indicates 90% confidence band, calculated from monthly means using ordinary least squares regression. Text indicates trend, with significance at the 90% confidence level (according to Student's t-test) indicated by bolding.

also has a notable seasonal cycle, increasing from a minimum of 3.6 mm in January to a maximum of 17.4 mm in June. Precipitable water vapor is also increasing – sunlit months increased by 0.63±0.36 mm/decade ($p < 0.01$) while dark months increased by 0.24±0.23 mm/decade ($p = 0.09$). While near-surface air temperature and precipitable water vapor increased, warming was greater during dark months while moistening was greater during sunlit months.

Surface albedo is increasing at ARM NSA during the sunlit season (Fig. 4j). This increase is embedded within a seasonal cycle that transitions from snow-covered (0.8) to bare (0.2) tundra in May-June back to snow-covered tundra in September-October (Fig. 4i). Surface albedo increases during July and August at ARM and NOAA sites (Fig. 5e,f) when bare tundra is exposed. No months show decreasing surface albedo. Melt-out and snow-in dates–which strongly impact surface albedo during transitional months–have no trend 2001-2023 in either ARM or NOAA data (Fig. 5a,b). This lack of change suggests that snow season timing changes do not contribute to the surface albedo trend. Instead, surface albedo increases during months when it is controlled by vegetation and surface water.

Cloud properties at ARM NSA are also changing. Annually, ARM NSA shows increasing cloud cover ($p = 0.06$), cloud liquid water path ($p < 0.01$), and low cloud fraction ($p < 0.01$) (Fig. 6 d, h, i). These increases occur primarily during sunlit months. Cloud liquid water path and low cloud fraction (relative to all clouds) increase during sunlit months ($p < 0.01$).

https://doi.org/10.5194/egusphere-2026-4740
Preprint. Discussion started: 28 August 2026

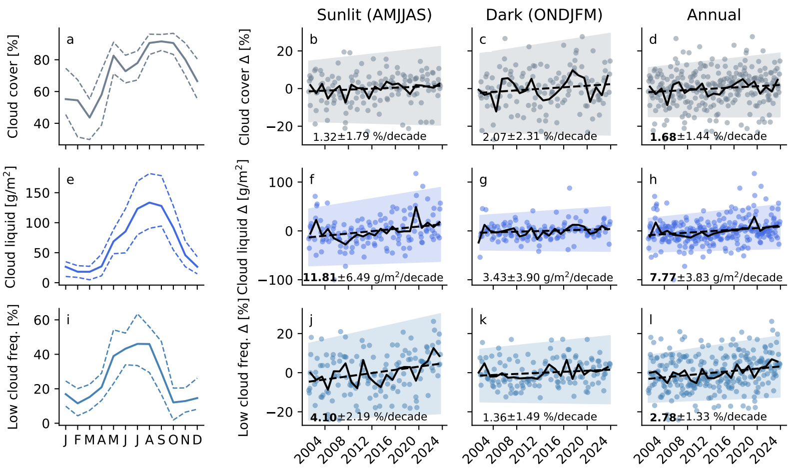

Figure 6. Same as Figure 4, but for cloud drivers. Cloud drivers are cloud cover, cloud liquid water path, and frequency of low cloud base heights (< 250 m) relative to all clouds.

Increasing cloud cover is more significant annually than during either dark or sunlit months. During dark months, cloud cover, liquid water path, and low cloud fraction all have weaker and insignificant increases ($p = 0.14, 0.15, 0.13$, respectively). Each cloud property change uniquely affects radiation based on climatological conditions, making for a seasonally-varying set of competing radiative impacts. In order to understand how much each change radiatively warms or cools the surface, further analysis is needed.

3.3 Radiation trend attribution

3.3.1 Reconstruction of observed trends

We now quantify what drove surface radiation trends 2001-2023 at ARM NSA. We find the radiative effect of monthly anomalies in each of the six assessed drivers–air temperature, greenhouse gases, surface albedo, cloud cover, liquid water path, low cloud fraction–individually. Through trend analysis of the reconstructed radiative anomaly time series (Fig. 7), we can identify which changes in radiatively important properties drove observed surface radiation trends.

Net shortwave radiation change was driven primarily by changing cloud properties and increasing surface albedo. The sum total of assessed cloud drivers had the largest impact, explaining -2.2 W/m^2/decade. Increasing surface albedo had a secondary but still substantial role, contributing -1.3 W/m^2/decade (Fig. A3). Increasing water vapor played a tertiary role, contributing -0.3 W/m^2/decade. Cumulatively, the reconstructed net shortwave radiation trend during sunlit months is -4.0±2.5 W/m^2/decade, consistent with the observed total of -4.7±3.0 W/m^2/decade. The sum total effect of these drivers is consistent with the observed total, giving us confidence in our ability to attribute shortwave radiation change.

In terms of downwelling longwave radiation, warming alone can explain less than half of the observed increase during both sunlit and dark months (Fig. 7d,f). During the dark season, atmospheric warming explains 3.4 out of the observed 8.2

https://doi.org/10.5194/egusphere-2026-4740
Preprint. Discussion started: 28 August 2026

W/m^2/decade longwave radiation increase. During the sunlit season, atmospheric warming explains 1.1 out of the observed 3.6 W/m^2/decade longwave radiation increase. While important, the radiative impact of increasing air temperature is only part of the overall radiation change.

The combined effects of changes in atmospheric temperature and greenhouse gases (water vapor and CO_2) explain roughly half of the magnitude of observed downwelling longwave radiation trends (Fig. 7j,l). On their own, increasing greenhouse gases (water vapor and CO_2) explain 0.99 W/m^2/decade of the downwelling longwave radiation trend during dark months and 1.07 W/m^2/decade during sunlit months. Increasing water vapor and air temperature have roughly equal impacts on increasing surface radiation during sunlit months. During dark months, greenhouse gas change has a smaller radiative effect than air temperature change due to its stronger warming. Water vapor is responsible for the overall greenhouse gas driving of surface downwelling longwave radiation change, since the effect of increasing water vapor is an order of magnitude larger than that of CO_2 (not shown). Still, non-cloud drivers alone are insufficient to explain the magnitude of downwelling longwave radiation change.

Including cloud property changes brings downwelling longwave radiation trends closer to observed totals. Changes in assessed cloud properties (cloud cover, cloud liquid water path, and low cloud fraction) explain 0.64 W/m^2/decade of the longwave radiation trend during sunlit months and 1.95 W/m^2/decade during dark months. This contribution increases the longwave radiation trend up to observed totals during sunlit months (3.3±1.9 of the total 3.6±2.0 W/m^2/decade trend). During dark months, however, the total attributed trend is too small. Only 5.6±2.8 out of the observed 8.2±3.1 W/m^2/decade trend is explained by the full set of assessed drivers, which cannot account for all cloud changes.

In contrast to all-sky longwave radiation, changing clear-sky radiation can be fully explained during dark months (Fig. 8). The observed clear-sky downwelling longwave radiation increase of 3.5±2.6 W/m^2/decade agrees well with the attributed total of 3.3±2.2 W/m^2/decade. As might be expected, atmospheric warming is the largest contributor with a small contribution from increasing water vapor. Air temperature and water vapor changes affect longwave radiation less strongly under clear-sky than all-sky conditions. For temperature, this weaker driving results from the decreased atmospheric emissivity without clouds in the lower layers of the atmosphere with the most warming. Conversely, the weaker effect of water vapor comes from a smaller increase in precipitable water vapor under clear-sky than all-sky conditions (not shown). Smaller observed trends and better closure for clear skies highlight the importance of cloud changes for downwelling longwave radiation change during dark months.

3.3.2 Cloud drivers of radiation trends

Three cloud properties were assessed as drivers (cloud cover, liquid water path, and low cloud fraction) and they had seasonally varying importance (Fig. 9). During dark months, changing liquid water path and cloud cover drove roughly equal increases in downwelling longwave radiation, while the impact of low cloud fraction was small. During sunlit months, the cloud contribution to increasing longwave radiation was driven by cloud cover and low cloud fraction changes. Despite increasing substantially during sunlit months, liquid water path change only drove a small longwave increase. This weaker effect was because of the greater frequency of blackbody clouds during sunlit months (liquid water path > 30 g/m^2, Figure 6i).

https://doi.org/10.5194/egusphere-2026-4740
Preprint. Discussion started: 28 August 2026

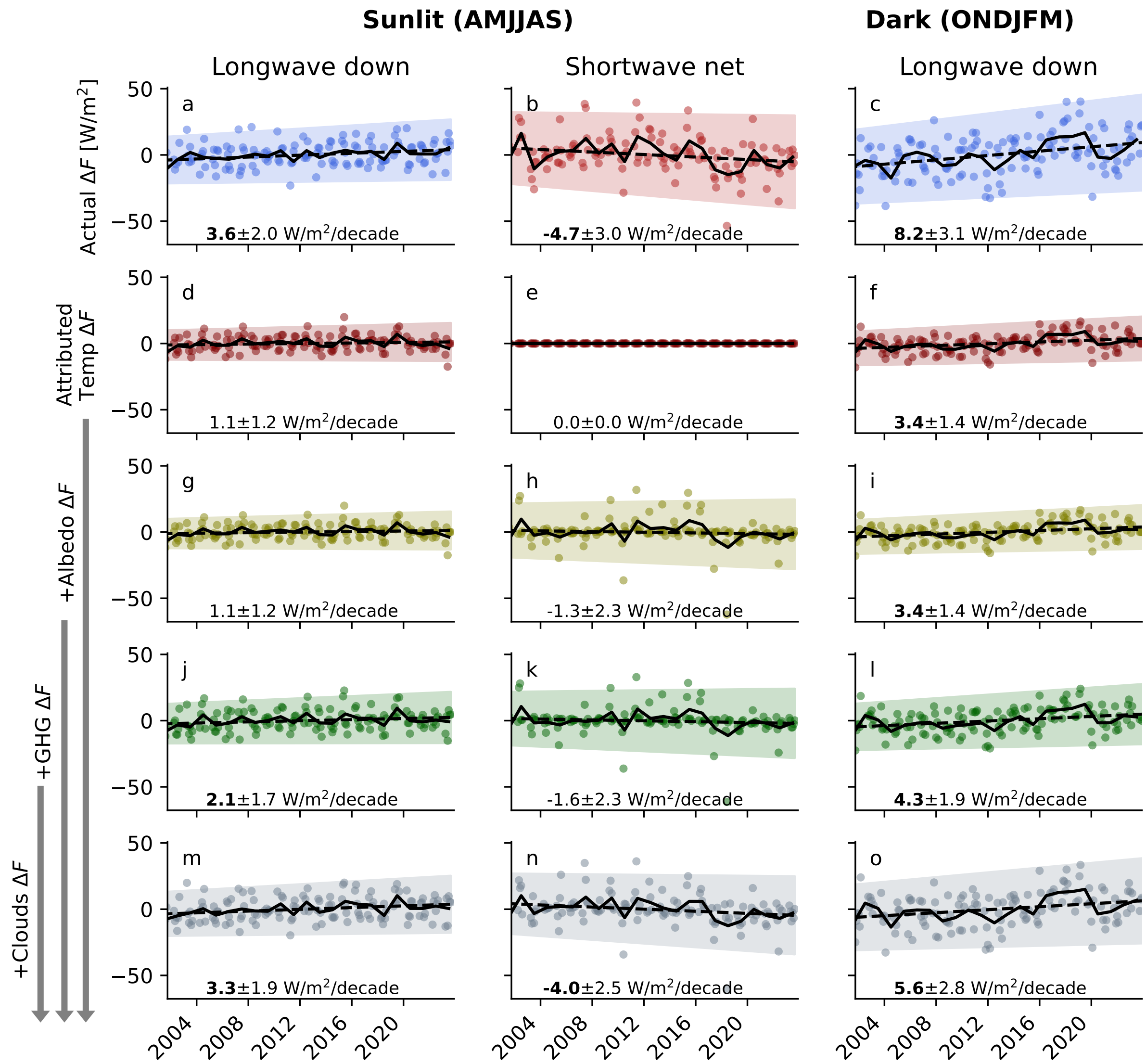

Figure 7. Observed (top row) and reconstructed (below) radiation trends from cumulative sums of observed driver anomalies. For sunlit months, downwelling longwave (left column) and net shortwave (second from left column) radiation are shown. For the dark months, only downwelling longwave (right column) is shown because net shortwave is negligible during this time. Drivers considered are temperature (d-f); surface albedo plus temperature (g-i); greenhouse gases (water vapor and CO_2) plus surface albedo and temperature (j-l); and the sum of clouds, greenhouse gases, surface albedo, and temperature (m-o). Markers indicate monthly-mean anomalies and solid line indicates seasonal (or annual) average. Line of best fit is indicated by dashed line and shaded area indicates 90% confidence band, calculated from monthly means using ordinary least squares regression. Text indicates trend, with significance at the 90% confidence level (according to Student's t-test) indicated by bolding.

https://doi.org/10.5194/egusphere-2026-4740
Preprint. Discussion started: 28 August 2026

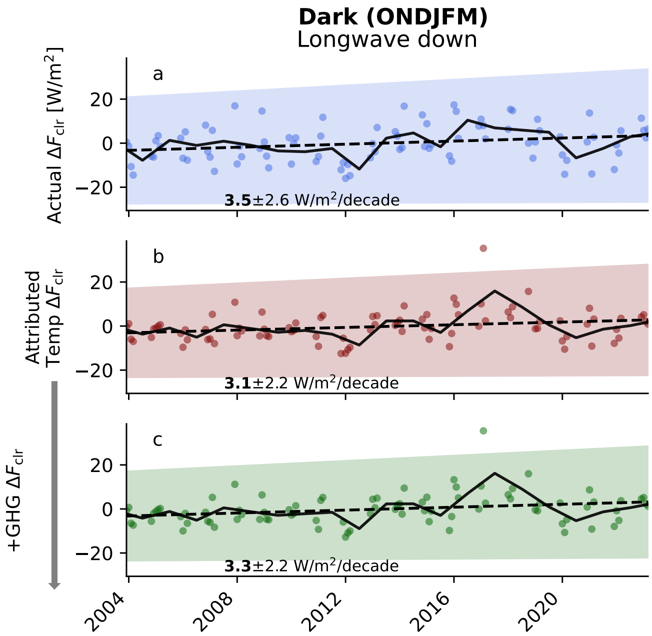

Figure 8. Observed (top row) and reconstructed (below) clear-sky radiation trends from cumulative sums of observed driver anomalies during dark months. Only dark months are shown due to infrequent clear-sky conditions during sunlit months. Drivers considered are temperature (b) and greenhouse gases (water vapor and CO_2) plus temperature (c). Markers indicate monthly-mean anomalies and solid line indicates seasonal average. Line of best fit is indicated by dashed line and shaded area indicates 90% confidence band, calculated from monthly means using ordinary least squares regression. Text indicates trend, with significance at the 90% confidence level (according to Student's t-test) indicated by bolding. Clear-sky conditions are determined using radiometric tests from Riihimaki et al. (2003).

In contrast, liquid water path and cloud cover drove decreasing shortwave radiation during sunlit months. However, cloud cover and liquid water path did not contribute equally. The shortwave radiative impact of increasing cloud cover was nearly twice as large as that of increasing liquid water path. But for both cloud cover and liquid water path, their longwave increase only partially offset the shortwave decrease. While much weaker due to longwave-shortwave cancellation, clouds drove a decrease in total radiation input during sunlit months.

Cloud-driven shortwave and longwave effects largely offset one another when considered across the full year. Annually, cloud cover and liquid water path changes drove a slight decrease in total radiation. The radiative effect of increasing low cloud fraction, however, is solely a longwave increase. Added together, the annual total radiative effect of all cloud changes is near-zero. The assessed cloud shortwave-driven decrease during sunlit months canceled out the cloud longwave-driven increase during dark months.

Clouds increasingly cool the surface during sunlit months and warm it during dark months, but it is not clear precisely when this transition occurs. Examining trends in cloud versus non-cloud radiative anomalies by meteorological season reveals its timing (Fig. 10): DJF and MAM cloud property changes increase total radiation input, while JJA cloud property changes

https://doi.org/10.5194/egusphere-2026-4740
Preprint. Discussion started: 28 August 2026

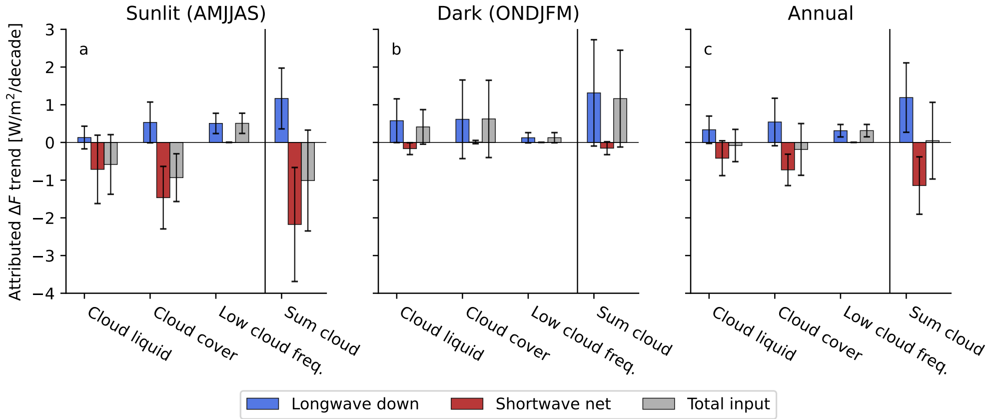

Figure 9. Surface radiation trend implied by anomalies in cloud cover, cloud liquid water path, low cloud fraction, and all drivers together during sunlit months (a), dark months (b), and annually (c). Radiation trend is shown for downwelling longwave, net shortwave, and total input (downwelling longwave plus net shortwave). Trend is calculated from monthly mean anomalies using ordinary least squares regression and error bars indicate 90% confidence interval diagnosed from Student's t-test.

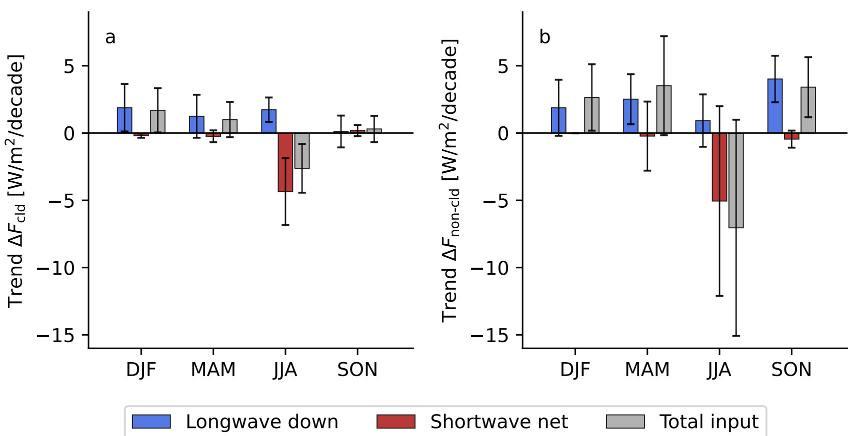

Figure 10. Trends 2001-2023 in cloud (a) vs. non-cloud (b) driven surface radiative anomalies by meteorological season. Radiative anomalies are shown for downwelling longwave, net shortwave, and total radiation (longwave plus shortwave). Trends calculated from ordinary least squares regression on monthly data. Error bars indicate 90% confidence interval diagnosed from Student's t-test.

320 decrease it. SON, by contrast, has no change in either longwave or shortwave assessed cloud radiative effect. This absence of cloud radiative effect change occurs despite substantial non-cloud radiation change during the same season (Fig. 10b). Taken together, these results show cloud-radiative driving transitioning from cooling in JJA, to no change in SON, to warming in DJF and MAM.

https://doi.org/10.5194/egusphere-2026-4740
Preprint. Discussion started: 28 August 2026

4 Discussion

Cloud changes at ARM NSA substantially modified the surface radiative effects of atmospheric warming and moistening. Depending on the time of year, cloud changes either doubled (dark months) or cancelled out (sunlit months) the longwave warming effects of changing water vapor and atmospheric temperature. However, the causes of observed cloud changes themselves remain unclear. In particular, the role of atmospheric circulation variability was not assessed in this study. Recent work (Lubin et al., 2026) has shown that increasing frequency of atmospheric rivers is one contributor to increasing liquid water path at ARM NSA. Thus some degree of circulation influence is already established, but a full explanation of the magnitude of changes is still needed.

Whatever radiative changes are not due to internally-generated climate variability would result from the Arctic response to external forcing. Quantitative detection of a response to external forcing can take much more than two decades of observations (e.g., Sledd and L'Ecuyer, 2021), making continued long-term observations invaluable. In the meantime, ESM simulations nudged to observed winds can enable meaningful model-observation comparison. If constrained to the circulation that ARM NSA actually observed, the ESM might be expected to reproduce observed changes and provide a unique avenue for model evaluation.

Beyond questions of circulation influence, several aspects of the driver analysis itself warrant further consideration–in particular surface albedo changes. A shortening of the snow year over tundra is an important contributor to longer-term changes in Arctic surface albedo as a whole (Chapin et al., 2005) and at Utqiagvik over 1979-2016 (Cox et al., 2017). Its absence over 2001-2023 cautions against temporally extrapolating reported changes and may be worth further exploration. When albedo does change, it increases at both sites due to either vegetation or surface water changes. This change is consistent with satellite observations of the North Slope as a whole and has been linked to increasing vegetation biomass (Plekhanova et al., 2022), though changing surface water may also play a role (Webb et al., 2021).

Additionally, cloud drivers should be explored further. Several radiatively important cloud properties were assessed – cloud liquid water path, low cloud fraction, and cloud cover – but several cloud properties remain unassessed. These unassessed cloud drivers may have an important effect on increasing downwelling longwave radiation during dark months. Their importance is suggested by the fact that the larger all-sky longwave increase was underestimated while the smaller clear-sky increase was not. In particular, the radiative effect of ice water path change was not assessed due to temporally limited observations. Previous studies over shorter time periods at ARM NSA (Sokolowsky et al., 2020; Bertrand et al., 2025) found that cloud ice variations have a substantial impact on longwave radiation, suggesting relevance to 2001-2023. In order to assess the impact of cloud ice changes on 23-year trends, future work should devise alternative ice water path or cloud phase retrievals with greater temporal coverage and consistency over time.

Furthermore, increasing low cloud fraction during sunlit months appeared to be significant. Low cloud fraction was not defined at the typical height of several kilometers because there was no clear relationship with longwave radiation. Instead, it was defined as base heights <250 m, which emphasizes surface fog. With this definition, low cloud fraction increases over

https://doi.org/10.5194/egusphere-2026-4740
Preprint. Discussion started: 28 August 2026

time and has a pronounced relationship with radiation via greater in-cloud temperatures. The causes of this increase over time and relationship with radiation should be understood at ARM NSA and elsewhere.

More generally, it remains an open question how applicable results at Utqiagvik are to the broader Arctic. Due to variations in surface cover type, the surface response to atmospheric radiative forcing (i.e., total radiation input) varies greatly between tundra and other surface types such as sea ice. Yet the reported changes in downwelling radiation originating from the atmosphere should be representative of some broader area. The part of the total radiation input which varies is surface albedo, and it determines whether longwave warming or shortwave cooling prevails. Comparing tundra to nearby ocean, the lower albedo of open water would drive greater reductions in net shortwave than was reported over land. Local sea ice observations may be useful in exploring the marine effects of reported atmospheric changes.

The reported change in total radiation input to the Utqiagvik sites is partitioned into several surface energy budget responses. Specifically, some combination of ground heat flux, turbulent fluxes, and surface skin temperature would adjust in response to decreasing radiation input. Considering that surface skin temperature at NOAA did not decrease in response to decreasing total radiation input during sunlit months, other surface energy budget terms might dominate the response.

5 Conclusions

In this study, we reported surface radiation trends 2001-2023 at the ARM North Slope of Alaska (NSA) facility and identified which atmospheric and surface property changes drove observed radiation trends. We found that increasing cloud liquid water path, cloud cover, and surface albedo drove decreasing net shortwave radiation during sunlit months (April-September). This decrease cancelled out the longwave effect of increasing water vapor and temperature, resulting in no change (ARM) or a decrease (NOAA) in total radiation input to the surface during sunlit months. During dark months, we found that warming and moistening alone could only explain half the magnitude of the observed increase in downwelling longwave radiation, suggesting a substantial role for increasing cloud radiative effect. While Arctic warming is a consistent response to external forcing, this study demonstrates how Arctic cloud changes strongly modulate 23-year trends in surface radiation to amplify or dampen warming depending on the season.

Overall, the drivers assessed here are sufficient to reconstruct the sign–and in most cases the magnitude–of observed radiation trends. Water vapor, temperature, surface albedo, cloud liquid water, and cloud cover observations are enough to reproduce observed increasing surface downwelling longwave radiation and decreasing surface net shortwave radiation. This consistency using novel analysis of observations underscores the robustness of existing physical understanding of Arctic change. Points of underestimation–specifically increasing downwelling longwave during dark months–highlight areas for future research.

Code and data availability. ARM datasets are available at the ARM data center (https://adc.arm.gov). RRTM is available on GitHub (github.com/AER-RC). See dataset citations for complete list.

https://doi.org/10.5194/egusphere-2026-4740
Preprint. Discussion started: 28 August 2026

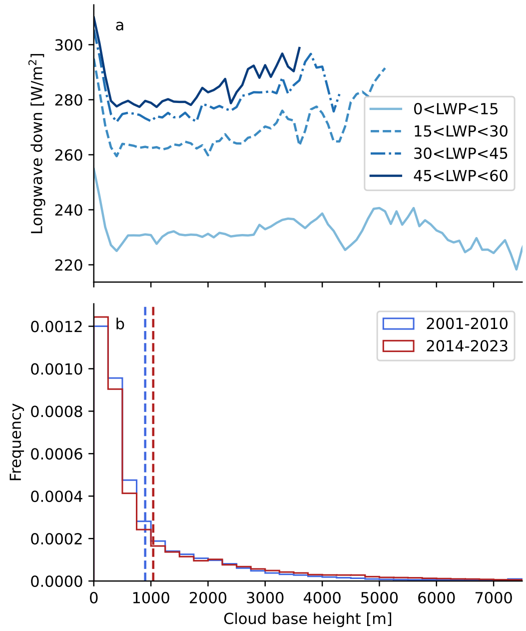

Figure A1. Ceilometer-derived lowest cloud base height relationship with downwelling longwave radiation (a) and cloud base height histogram and average (vertical line) by decade (b). Average downwelling longwave for all observations of a given cloud base height (a) are stratified by liquid water path (LWP) to ensure sampling of similar-opacity clouds. Average downwelling longwave for a given cloud base height and liquid water path is only shown when over 500 observations are available. Histograms (b) are shown for the first and last decade of observations.

Appendix A: Appendix

Author contributions. LB wrote the manuscript, conducted analysis, and prepared figures. JEK and GdB reviewed the manuscript and assisted with interpretation. LB and JEK were supported by NASA PREFIRE mission award 849K995. LB was additionally supported by the Cooperative Institute for Research in Environmental Sciences (CIRES) at the University of Colorado.

Competing interests. The authors declare that no competing interests are present.

Acknowledgements. This work was supported by the NASA PREFIRE Mission (Award 849K995, JEK and LB) and by an award to LB from the CIRES Graduate Student Research Award Program. This work utilized the Alpine high-performance-computing resource at the University of Colorado Boulder. Alpine is jointly funded by the University of Colorado Boulder, the University of Colorado Anschutz,

https://doi.org/10.5194/egusphere-2026-4740
Preprint. Discussion started: 28 August 2026

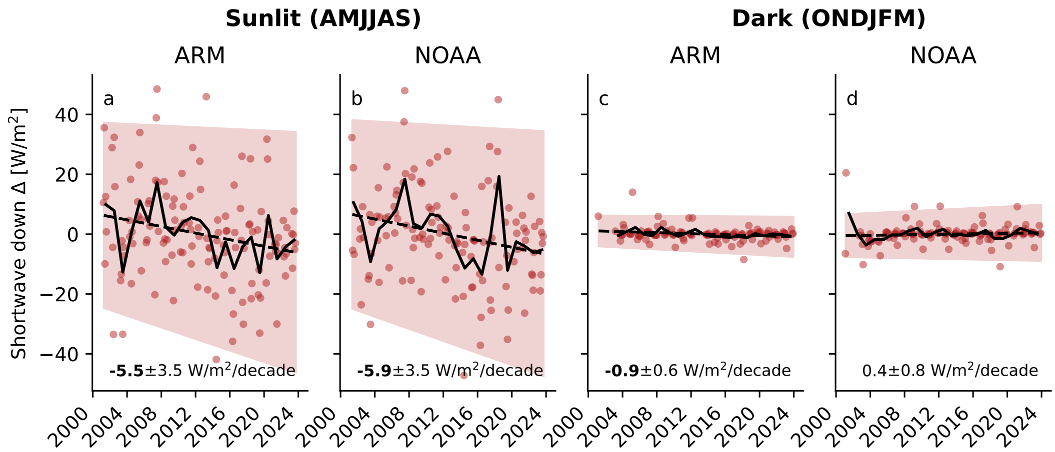

Figure A2. Like Figure 2, but for surface downwelling shortwave radiation.

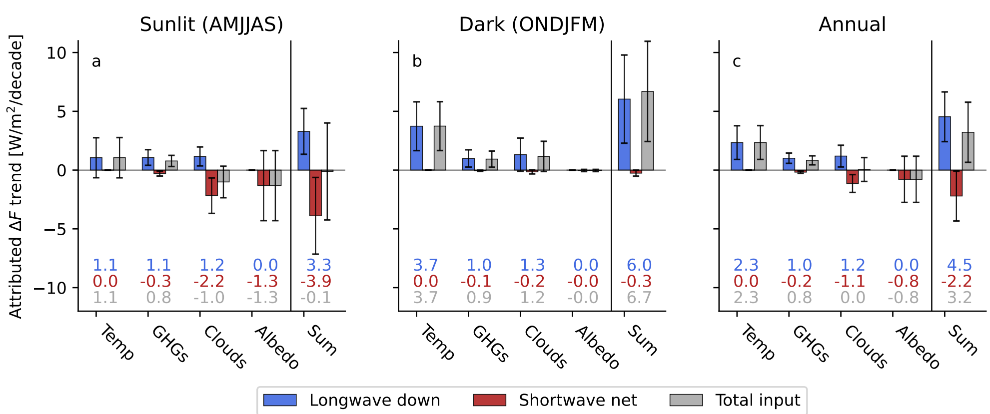

Figure A3. Surface radiation trend implied by anomalies in temperature, greenhouse gases (GHGs), clouds, albedo, and all drivers together. Radiation trend is shown for downwelling longwave, net shortwave, and total radiative input. Text indicates average slope of regression in W/m^2/decade. Trend is calculated from monthly mean anomalies using ordinary least squares regression. Error bars indicate 90% confidence interval diagnosed from Student's t-test.

https://doi.org/10.5194/egusphere-2026-4740
Preprint. Discussion started: 28 August 2026

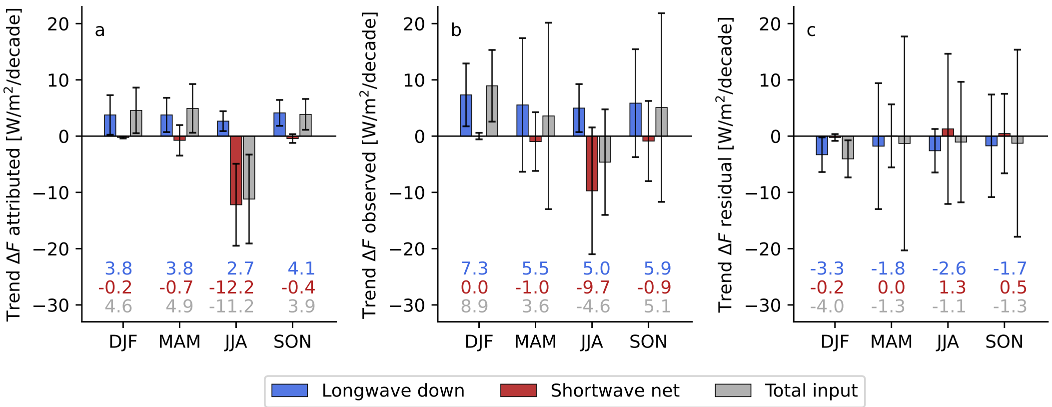

Figure A4. Surface radiation trend radiative closure by meteorological season. Trends in downwelling longwave radiation, net shortwave radiation, and their sum for attributed total flux anomalies (a), directly observed flux anomalies (b), and attributed minus observed (c). Text indicates average slope of regression in W/m^2/decade. Trends calculated from ordinary least squares regression on monthly data. Error bars indicate 90% confidence interval diagnosed from Student's t-test.

Colorado State University, and the National Science Foundation (Award 2201538). The authors wish to thank Prof. Matthew Shupe and Prof. John Cassano for providing feedback on the manuscript. The authors also wish to thank Dr. Laura Riihimaki, Dr. Christopher Cox, and Dr. David Clemens-Sewall for helpful discussions on shortwave radiation observations and Dr. Damao Zhang for handling ARM data processing requests.

https://doi.org/10.5194/egusphere-2026-4740
Preprint. Discussion started: 28 August 2026

References

Barrientos-Velasco, C., Cox, C. J., Deneke, H., Dodson, J. B., Hünerbein, A., Shupe, M. D., Taylor, P. C., and Macke, A.: Estimation of the Radiation Budget during MOSAiC Based on Ground-Based and Satellite Remote Sensing Observations, Atmospheric Chemistry and Physics, 25, 3929–3960, https://doi.org/10.5194/acp-25-3929-2025, 2025.

Bertossa, C. and L'Ecuyer, T.: A Rapid Deterioration of the Transmissive Atmospheric Radiative Regime in the Western Arctic, Geophysical Research Letters, 52, e2025GL115 362, https://doi.org/10.1029/2025GL115362, 2025.

Bertrand, L., Kay, J. E., and De Boer, G.: Increasing Wintertime Cloud Opacity Increases Surface Longwave Radiation at a Long-Term Arctic Observatory, Nature Communications, 16, 9135, https://doi.org/10.1038/s41467-025-64441-8, 2025.

Ceppi, P., McCoy, D. T., and Hartmann, D. L.: Observational Evidence for a Negative Shortwave Cloud Feedback in Middle to High Latitudes, Geophysical Research Letters, 43, 1331–1339, https://doi.org/10.1002/2015GL067499, 2016.

Chapin, F. S., Sturm, M., Serreze, M. C., McFadden, J. P., Key, J. R., Lloyd, A. H., McGuire, A. D., Rupp, T. S., Lynch, A. H., Schimel, J. P., Beringer, J., Chapman, W. L., Epstein, H. E., Euskirchen, E. S., Hinzman, L. D., Jia, G., Ping, C.-L., Tape, K. D., Thompson, C. D. C., Walker, D. A., and Welker, J. M.: Role of Land-Surface Changes in Arctic Summer Warming, Science, 310, 657–660, https://doi.org/10.1126/science.1117368, 2005.

Clough, S., Shephard, M., Mlawer, E., Delamere, J., Iacono, M., Cady-Pereira, K., Boukabara, S., and Brown, P.: Atmospheric Radiative Transfer Modeling: A Summary of the AER Codes, Journal of Quantitative Spectroscopy and Radiative Transfer, 91, 233–244, https://doi.org/10.1016/j.jqsrt.2004.05.058, 2005.

Cox, C. J., Stone, R. S., Douglas, D. C., Stanitski, D. M., Divoky, G. J., Dutton, G. S., Sweeney, C., George, J. C., and Longenecker, D. U.: Drivers and Environmental Responses to the Changing Annual Snow Cycle of Northern Alaska, Bulletin of the American Meteorological Society, 98, 2559–2577, https://doi.org/10.1175/BAMS-D-16-0201.1, 2017.

Dong, X., Xi, B., Crosby, K., Long, C. N., Stone, R. S., and Shupe, M. D.: A 10 Year Climatology of Arctic Cloud Fraction and Radiative Forcing at Barrow, Alaska, Journal of Geophysical Research, 115, D17 212, https://doi.org/10.1029/2009JD013489, 2010.

Graham, R. M., Rinke, A., Cohen, L., Hudson, S. R., Walden, V. P., Granskog, M. A., Dorn, W., Kayser, M., and Maturilli, M.: A Comparison of the Two Arctic Atmospheric Winter States Observed during N-ICE2015 and SHEBA, Journal of Geophysical Research: Atmospheres, 122, 5716–5737, https://doi.org/10.1002/2016JD025475, 2017.

Huang, Y., Taylor, P. C., Rose, F. G., Rutan, D. A., Shupe, M. D., Webster, M. A., and Smith, M. M.: Toward a More Realistic Representation of Surface Albedo in NASA CERES-derived Surface Radiative Fluxes, Elementa: Science of the Anthropocene, 10, 00 013, https://doi.org/10.1525/elementa.2022.00013, 2022.

Korolev, A., McFarquhar, G., Field, P. R., Franklin, C., Lawson, P., Wang, Z., Williams, E., Abel, S. J., Axisa, D., Borrmann, S., Crosier, J., Fugal, J., Krämer, M., Lohmann, U., Schlenczek, O., Schnaiter, M., and Wendisch, M.: Mixed-Phase Clouds: Progress and Challenges, vol. 58, https://doi.org/10.1175/AMSMONOGRAPHS-D-17-0001.1, 2017.

Kyrouac, J., Shi, Y., and Tuftedal, M.: Surface Meteorological Instrumentation (MET), https://doi.org/10.5439/1786358, north Slope Alaska (NSA), Central Facility, Barrow AK (C1), 2003.

Liu, X., He, T., Sun, L., Xiao, X., Liang, S., and Li, S.: Analysis of Daytime Cloud Fraction Spatiotemporal Variation over the Arctic from 2000 to 2019 from Multiple Satellite Products, Journal of Climate, 35, 7595–7623, https://doi.org/10.1175/JCLI-D-22-0007.1, 2022.

https://doi.org/10.5194/egusphere-2026-4740
Preprint. Discussion started: 28 August 2026

Liu, Y., Shupe, M. D., Wang, Z., and Mace, G.: Cloud Vertical Distribution from Combined Surface and Space Radar–Lidar Observations at Two Arctic Atmospheric Observatories, Atmospheric Chemistry and Physics, 17, 5973–5989, https://doi.org/10.5194/acp-17-5973-2017, 2017.

Long, C. N. and Shi, Y.: The QCRad Value Added Product: Surface Radiation Measurement Quality Control Testing, Including Climatology Configurable Limits (Report No. DOE/SC-ARM/TR-074, U.S. Department of Energy, Office of Science, Office of Biological and Environmental Research, https://www.arm.gov/publications/tech_reports/doe-sc-arm-tr-074.pdf, 2006.

Lubin, D., Zou, X., Mülmenstädt, J., Vogelmann, A., Cadeddu, M., and Zhang, D.: Surface Radiation Trends at North Slope of Alaska Influenced by Large-Scale Circulation and Atmospheric Rivers, Atmospheric Chemistry and Physics, 26, 295–311, https://doi.org/10.5194/acp-26-295-2026, 2026.

Maturilli, M., Herber, A., and König-Langlo, G.: Surface Radiation Climatology for Ny-Ålesund, Svalbard (78.9° N), Basic Observations for Trend Detection, Theoretical and Applied Climatology, 120, 331–339, https://doi.org/10.1007/s00704-014-1173-4, 2015.

Miller, N. B., Shupe, M. D., Cox, C. J., Noone, D., Persson, P. O. G., and Steffen, K.: Surface Energy Budget Responses to Radiative Forcing at Summit, Greenland, The Cryosphere, 11, 497–516, https://doi.org/10.5194/tc-11-497-2017, 2017.

Mlawer, E. J., Taubman, S. J., Brown, P. D., Iacono, M. J., and Clough, S. A.: Radiative Transfer for Inhomogeneous Atmospheres: RRTM, a Validated Correlated-k Model for the Longwave, Journal of Geophysical Research: Atmospheres, 102, 16 663–16 682, https://doi.org/10.1029/97JD00237, 1997.

Morris, V., Zhang, D., and Ermold, B.: Ceilometer (CEIL), https://doi.org/10.5439/1181954, north Slope Alaska (NSA) Central Facility, Barrow AK (C1), 1997.

Plekhanova, E., Kim, J.-S., Oehri, J., Erb, A., Schaaf, C., and Schaepman-Strub, G.: Mid-Summer Snow-Free Albedo across the Arctic Tundra Was Mostly Stable or Increased over the Past Two Decades, Environmental Research Letters, 17, 124 026, https://doi.org/10.1088/1748-9326/aca5a1, 2022.

Riihimaki, L., Zhang, D., and Gaustad, K.: Radiative Flux Analysis (RADFLUX1LONG), North Slope Alaska (NSA), Central Facility, Barrow AK (C1), https://doi.org/10.5439/1395157, 2003.

Riot-Bretêcher, B., Huang, Y., Liu, L., and Gero, J.: Strengthening Atmospheric Greenhouse Effect at the Arctic North Slope of Alaska Site Evidenced by Long-Term Records of the Downwelling Longwave Radiance Spectrum, Journal of Geophysical Research: Atmospheres, 130, e2025JD043 680, https://doi.org/10.1029/2025JD043680, 2025.

Rosenlof, K., Hassler, B., Bodeker, G., and NOAA CDR Program: NOAA Climate Data Record (CDR) of Zonal Mean Ozone Binary Database of Profiles (BDBP), Version 1.0, https://doi.org/10.7289/V56M34RT, 2015.

Screen, J. A., Deser, C., and Simmonds, I.: Local and Remote Controls on Observed Arctic Warming, Geophysical Research Letters, 39, 2012GL051 598, https://doi.org/10.1029/2012GL051598, 2012.

Shupe, M. D. and Intrieri, J. M.: Cloud Radiative Forcing of the Arctic Surface: The Influence of Cloud Properties, Surface Albedo, and Solar Zenith Angle, Journal of Climate, 17, 616–628, https://doi.org/10.1175/1520-0442(2004)017<0616:CRFOTA>2.0.CO;2, 2004.

Shupe, M. D., Turner, D. D., Zwink, A., Thieman, M. M., Mlawer, E. J., and Shippert, T.: Deriving Arctic Cloud Microphysics at Barrow, Alaska: Algorithms, Results, and Radiative Closure, Journal of Applied Meteorology and Climatology, 54, 1675–1689, https://doi.org/10.1175/JAMC-D-15-0054.1, 2015.

Sledd, A. and L'Ecuyer, T.: Uncertainty in Forced and Natural Arctic Solar Absorption Variations in CMIP6 Models, Journal of Climate, 34, 931–948, https://doi.org/10.1175/JCLI-D-20-0244.1, 2021.

https://doi.org/10.5194/egusphere-2026-4740
Preprint. Discussion started: 28 August 2026

Sledd, A., Shupe, M. D., Solomon, A., and Cox, C. J.: Surface Energy Balance Responses to Radiative Forcing in the Central Arctic From MOSAiC and Models, Journal of Geophysical Research: Atmospheres, 130, e2024JD042 578, https://doi.org/10.1029/2024JD042578, 2025.

Smith, N. and Barnet, C. D.: CLIMCAPS—A NASA Long-Term Product for Infrared + Microwave Atmospheric Soundings, Earth and Space Science, 10, e2022EA002 701, https://doi.org/10.1029/2022EA002701, 2023.

Sokolowsky, G. A., Clothiaux, E. E., Baggett, C. F., Lee, S., Feldstein, S. B., Eloranta, E. W., Cadeddu, M. P., Bharadwaj, N., and Johnson, K. L.: Contributions to the Surface Downwelling Longwave Irradiance during Arctic Winter at Utqiaġvik (Barrow), Alaska, Journal of Climate, 33, 4555–4577, https://doi.org/10.1175/JCLI-D-18-0876.1, 2020.

Solomon, A., Shupe, M. D., Svensson, G., Barton, N. P., Batrak, Y., Bazile, E., Day, J. J., Doyle, J. D., Frank, H. P., Keeley, S., Remes, T., and Tolstykh, M.: The Winter Central Arctic Surface Energy Budget: A Model Evaluation Using Observations from the MOSAiC Campaign, Elem Sci Anth, 11, 00 104, https://doi.org/10.1525/elementa.2022.00104, 2023.

Stephens, G. L.: Radiation Profiles in Extended Water Clouds. II: Parameterization Schemes, Journal of the Atmospheric Sciences, 35, 2123–2132, https://doi.org/10.1175/1520-0469(1978)035<2123:RPIEWC>2.0.CO;2, 1978.

Stone, R. S., Dutton, E. G., Harris, J. M., and Longenecker, D.: Earlier Spring Snowmelt in Northern Alaska as an Indicator of Climate Change, Journal of Geophysical Research: Atmospheres, 107, https://doi.org/10.1029/2000JD000286, 2002.

Stroeve, J. C., Serreze, M. C., Holland, M. M., Kay, J. E., Malanik, J., and Barrett, A. P.: The Arctic's Rapidly Shrinking Sea Ice Cover: A Research Synthesis, Climatic Change, 110, 1005–1027, https://doi.org/10.1007/s10584-011-0101-1, 2012.

Turner, D. D., Vogelmann, A. M., Austin, R. T., Barnard, J. C., Cady-Pereira, K., Chiu, J. C., Clough, S. A., Flynn, C., Khaiyer, M. M., Liljegren, J., Johnson, K., Lin, B., Long, C., Marshak, A., Matrosov, S. Y., McFarlane, S. A., Miller, M., Min, Q., Minimis, P., O'Hirok, W., Wang, Z., and Wiscombe, W.: Thin Liquid Water Clouds: Their Importance and Our Challenge, Bulletin of the American Meteorological Society, 88, 177–190, https://doi.org/10.1175/BAMS-88-2-177, 2007.

Verlinde, J., Zak, B. D., Shupe, M. D., Ivey, M. D., and Stamnes, K.: The ARM North Slope of Alaska (NSA) Sites, Meteorological Monographs, 57, 8.1–8.13, https://doi.org/10.1175/AMSMONOGRAPHS-D-15-0023.1, 2016.

Wang, G., Wang, T., and Xue, H.: Validation and Comparison of Surface Shortwave and Longwave Radiation Products over the Three Poles, International Journal of Applied Earth Observation and Geoinformation, 104, 102 538, https://doi.org/10.1016/j.jag.2021.102538, 2021.

Webb, E. E., Loranty, M. M., and Lichstein, J. W.: Surface Water, Vegetation, and Fire as Drivers of the Terrestrial Arctic-boreal Albedo Feedback, Environmental Research Letters, 16, 084 046, https://doi.org/10.1088/1748-9326/ac14ea, 2021.

Wu, W., Sun, X., Epstein, H., Xu, X., and Li, X.: Spatial Heterogeneity of Climate Variation and Vegetation Response for Arctic and High-Elevation Regions from 2001–2018, Environmental Research Communications, 2, 011 007, https://doi.org/10.1088/2515-7620/ab6369, 2020.

Zelinka, M. D., Myers, T. A., McCoy, D. T., Po-Chedley, S., Caldwell, P. M., Ceppi, P., Klein, S. A., and Taylor, K. E.: Causes of Higher Climate Sensitivity in CMIP6 Models, Geophysical Research Letters, 47, e2019GL085 782, https://doi.org/10.1029/2019GL085782, 2020.

Zhang, D.: Data Quality Assessment for ARM Radiation Data (QCRAD1LONG), https://doi.org/10.5439/1227214, north Slope Alaska (NSA) Central Facility, Barrow AK (C1), 1998.

Zhang, D.: MWR Retrievals (MWRRET1LILJCLOU), https://doi.org/10.5439/1027369, north Slope Alaska (NSA) Central Facility, Barrow AK (C1), 2002.

https://doi.org/10.5194/egusphere-2026-4740
Preprint. Discussion started: 28 August 2026

Zhou, C., Liu, Y., and Wang, Q.: Calculating the Climatology and Anomalies of Surface Cloud Radiative Effect Using Cloud Property Histograms and Cloud Radiative Kernels, Advances in Atmospheric Sciences, 39, 2124–2136, https://doi.org/10.1007/s00376-021-1166-z, 2022.

Zhou, W., Leung, L. R., and Lu, J.: Steady Threefold Arctic Amplification of Externally Forced Warming Masked by Natural Variability, Nature Geoscience, 17, 508–515, https://doi.org/10.1038/s41561-024-01441-1, 2024.